Manipulating the *L*-valley electron *g* factor in Si-Ge heterostructures

F. A. Baron,[1] A. A. Kiselev,[2,*] H. D. Robinson,[1] K. W. Kim,[2] K. L. Wang,[1] and E. Yablonovitch[1]

[1]*University of California at Los Angeles, Los Angeles, California 90095, USA*
[2]*Department of Electrical and Computer Engineering, North Carolina State University, Raleigh, North Carolina 27695-7911, USA*
(Received 2 June 2003; published 6 November 2003)

The Zeeman effect for the *L* valley conduction band electrons in SiGe heterostructures is considered. A detailed calculation of the electron *g* tensor is performed in the framework of a relevant $\boldsymbol{k} \cdot \boldsymbol{p}$ model, developed specifically for the *L* point of the Brillouin zone. Electrons at the *L* point are considered under the influence of the different crystallographic orientations, alloy composition, quantum confinement, strain, and electric field, whose interplay causes a considerable deviation of the *g* tensor components from their bulk values. Our result strongly suggests that the SiGe-based quantum wells are a promising choice for the *g* tensor engineering for spin manipulation.

PACS number(s): 71.70.Ej, 75.30.Gw, 71.18.+y

I. INTRODUCTION

An ability to *in situ* control the electron Lande *g* tensor in the solid state is considered by many an important prerequisite for the practical manipulation of individual electron spins.[1–3] A suggestion that such a manipulation can be most easily realized in the SiGe-based heterostructures and particularly SiGe quantum dots,[4] is also gaining support. Thus, a theoretical guidance is needed for the early experiments in this field (and ultimately for the actual device fabrication).

To begin, let us speculate about the situation, suggested in Ref. 4. Assume that we have a layered SiGe heterostructure where lowest electron states in two adjacent layers are formed from *X* (Si-rich layer) and *L* (Ge-rich) valley states, respectively. We can apply electric field and use it to partially shift the electron wave function through the interface. Thus the question of how to calculate electron *g* factor for the whole heterostructure arises. Simple averaging $\boldsymbol{g} = \boldsymbol{g}_X w_{\mathrm{Si}} + \boldsymbol{g}_L w_{\mathrm{Ge}}$ of the *X* and *L* bulk *g* factors with probabilities w_{Si} and w_{Ge} to find electron in the Si- and Ge-rich layers is not adequate.

Instead, one should first calculate ground electron states in the biased structure separately for both *L* and *X* valleys, and compare their eigenstate energies. If the *X* state is lower, the answer for the whole heterostructure *g* factor is $\boldsymbol{g}_X$, calculated for the quantum-confined *X* state. Otherwise, one should focus on the *g* tensor for the quantum-confined *L* state. In the very narrow interval of parameters where energies E_L and E_X of the quantized levels are very close, one needs to consider microscopic properties of the heterointerface between two layers and evaluate small intervalley mixing potential V_{X-L}. After that, one must solve a two-level problem with the Hamiltonian

$$\hat{H} = \begin{pmatrix} E_X & V_{X\text{-}L} \\ V_{X\text{-}L}^* & E_L \end{pmatrix}$$

in order to find out the probability $w_X(w_L)$ for the electron in the whole system to have *X* (*L*) character. The "final" answer is

$$\boldsymbol{g} = \boldsymbol{g}_X w_X + \boldsymbol{g}_L w_L.$$

The evaluation of the intervalley mixing potential is beyond the scope of the present paper, but we will provide in-depth recipes for the calculation of $\boldsymbol{g}_L$ (calculation of $\boldsymbol{g}_X$ turns out to be trivial, see below).

The Zeeman effect at the *X* and *L* points in bulk Si and Ge was originally considered by Roth.[5] Extensions followed promptly by allowing refinement of the model, discriminating contributions of individual bands and their symmetry classes, etc. (see, for example, Ref. 6). Apart from the always existing free electron contribution ($g_0 \approx 2$), the electron effective Lande factor in a particular valley depends strongly on the *direct* energy gaps to the nearby spin-split bands (evaluated at the valley minimum in the *k* space) and the strength of these spin-orbit (SO) splittings.

For the *X* electron (or, actually, Δ in the vicinity of the *X* point) the situation is quite simple. It happens that the gaps with all the relevant bands are large. It was also pointed out that the spin splitting for the most important valence band vanishes exactly at the *X* point and is consequently small in its vicinity; the same can be found for the relevant p_z momentum matrix element.[5] As a result, the spin-orbit correction to the free electron value g_0 is universally small for the X (Δ) electrons, not only in the diamondlike semiconductors but also in the zinc blende–type III-V compounds and their respective heterostructures.[7] Thus, to a rather good accuracy one can conclude that for any X (Δ) electron, bulk or quantum confined, its *g* factor is approximately isotropic (in contrast to the effective mass tensor) and equal to g_0. For Si, this statement is additionally strengthened by the extreme intrinsic smallness of the SO interaction.

It was also established, both theoretically[5,6] and experimentally,[8,9] that the *g* factor of the bulk *L* electron is highly anisotropic (just like the effective mass) and can be characterized by the two components $g_\parallel$ and $g_\perp$ responsible for the directions parallel and perpendicular to the *L* axis, respectively. However, experiments would often deliver an average of the *g* factor tensor over all four (or some) of the equivalent *L* valleys. For example, for the ground donor state the symmetric superposition of the electron wave functions in all four *L* valleys makes the *g* factor isotropic. Luckily, the valley equivalence can be easily disturbed by strain, electric field, etc.
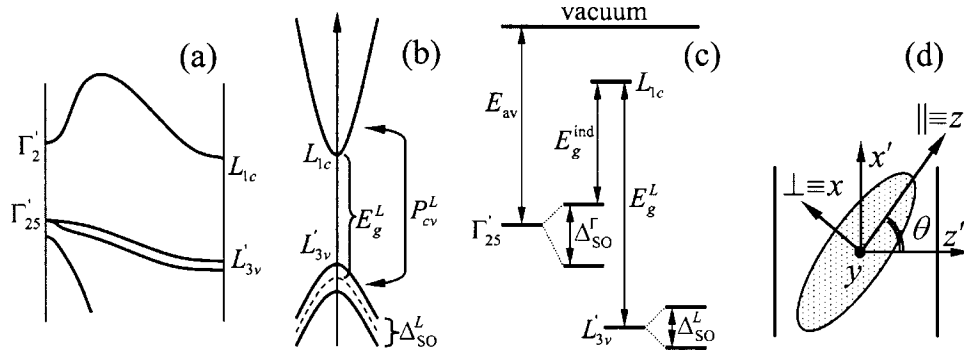
FIG. 1. Band structure of a diamond-type semiconductor at the L point. (a) Dispersion of the lowest conduction (Γ'_2-L_{1c}) and upper valence bands (Γ'_{25}-L'_{3v}) along the (111) direction. The SO splitting of the valence states is also sketched. (b) Dispersion of the L_{1c} and L'_{3v} electron states in the vicinity of the L point—shown for the (111) plane. (c) Energy diagram introducing important gaps and the vacuum level, suitable (in the first approximation) for the definition of the band offsets in the layered structures. (d) Coordinate systems (x,y,z) and (x',y,z') associated with the L valley and heterostructure, respectively.

Qualitatively, it is natural to expect that quantum confinement, strain, electric field in the low-dimensional SiGe heterostructures will result in further renormalization of the L electron g tensor. To our knowledge, no theoretical treatment of this problem was provided so far, unlike the Γ electron in zinc blende– and wurzitelike III-V and II-VI heterostructures.[10–14] We fill this gap with the present analysis.

The rest of the paper is organized as follows. First, we introduce a two-band $\boldsymbol{k}\cdot\boldsymbol{p}$ Kane-like model suitable for the description of the confined L valley electrons in SiGe heterostructures (Sec. II), accompanied by the analysis of the L electron quantum-confined states in the QW with both infinite and finite interface offsets. In Sec. III we provide a general recipe for the calculation of the Lande tensor and, for the particular case of the L electron in the QW heterostructures, derive closed expressions for three most important directions of the external magnetic field. We have made an attempt to collect available band structure data for SiGe heterostructures, which we discuss in Sec. IV. In Sec. V we analyze and numerically evaluate effects of the spacial confinement, crystallographic orientation, structure composition, electric field, etc., on the L electron g factor. We conclude with a short summary.

II. $\boldsymbol{k}\cdot\boldsymbol{p}$ MODEL FOR L VALLEY ELECTRONS

Figure 1(a) shows a dispersion of the lowest conduction (Γ'_2-L_{1c}) and upper valence bands (Γ'_{25}-L'_{3v}) along the (111) direction of the Brillouin zone (we use the classical notation by Herman[15]). It happens that all other bands are separated by substantial energy gaps at the L point. This fact offers an opportunity to introduce a rather simple two-band model description of the L_{1c} electron states in heterostructures (the same approximation was extensively discussed in relation to the Ge and Si bulk properties previously[5,6]). To begin the analysis, we represent the electron wave function Ψ in the form

$$\Psi = \hat{u}|L_{1c}\rangle + \hat{v}_x|L'^{\,x}_{3v}\rangle + \hat{v}_y|L'^{\,y}_{3v}\rangle,$$

where $\hat{u}$ and $\hat{v}_x, \hat{v}_y$ are spinor envelope functions in the conduction and valence bands, respectively. Two states of the upper valence band L'_{3v} would be degenerate in the absence of the SO interaction.

Now the general multiband $\boldsymbol{k}\cdot\boldsymbol{p}$ Hamiltonian $H(\boldsymbol{k})$ reduces to a 6×6 matrix. In terms of $\hat{u}$ and $\hat{v}_x, \hat{v}_y$, the Schrödinger equation for the state with energy E can be conveniently written as

$$E\hat{u} = (1/2 + F_{\text{remote}})k^2\hat{u} - iPk_x\hat{v}_x - iPk_y\hat{v}_y,$$

$$(E + E_g)\hat{v}_x = iPk_x\hat{u} - i\frac{\delta}{2}\hat{\sigma}_z\hat{v}_y,$$

$$(E + E_g)\hat{v}_y = iPk_y\hat{u} + i\frac{\delta}{2}\hat{\sigma}_z\hat{v}_x. \qquad (1)$$

Here the directions x,y,z are associated with the principal axes of a particular L valley, $z = (111)$ or equivalent; E_g is the direct energy gap at the L point L_{1c}-L'_{3v} (defined neglecting the SO interaction); δ is the SO splitting of the L'_{3v} valence band; P is the momentum matrix element; and $\hat{\sigma}_\alpha$ are the Pauli matrices.

Thus, the proposed two-band model [see Fig. 1(b) for a visual guide] accounts explicitly and fully for the $\boldsymbol{k}\cdot\boldsymbol{p}$ mixing between the lowest conduction states L_{1c} and upper valence states L'_{3v}. In an attempt to mimic the L_{1c} dispersion better, we have additionally included into the electron Hamiltonian a kinetic term with the free electron mass (which is 1 in atomic units that we use hereafter) as well as the approximate contribution from all other bands. These bands are treated as remote (due to much larger bandgaps as mentioned above), so their contribution is included (i) only for the conduction states (addition of similar terms into the valence band would produce minimal influence on the L_{1c} parameters) and (ii) in a quadratic-in-k approximation. Altogether, this results in a correction $2F_{\text{remote}}$ to the L_{1c} inverse mass tensor $\boldsymbol{m}^{-1}$ (as well as a correction to the Lande tensor $\Delta\boldsymbol{g}_{\text{remote}}$).

With the help of Eq. (1), the valence-band spinors $\hat{v}_x, \hat{v}_y$ can be expressed via the conduction-band spinor $\hat{u}$ as follows:

$$P\hat{v}_x = iAk_x\hat{u} - \hat{\sigma}_z Dk_y\hat{u},$$

$$P\hat{v}_y = iAk_y\hat{u} + \hat{\sigma}_z Dk_x\hat{u}, \qquad (2)$$

where

$$A = \frac{P^2}{2}\left(\frac{1}{E+E_g-\delta/2} + \frac{1}{E+E_g+\delta/2}\right),$$

$$D = -\frac{P^2}{2}\left(\frac{1}{E+E_g-\delta/2} - \frac{1}{E+E_g+\delta/2}\right). \qquad (3)$$

We would like to specifically note that the coefficients A and D are energy-dependent.

The dispersion equation for the spinor $\hat{u}$ in the heterostructure now takes a form

$$\{\mathbf{k}\cdot\boldsymbol{\mu}\cdot\mathbf{k} - i\hat{\sigma}_z(k_x Dk_y - k_y Dk_x) + (V-E)\}\hat{u} = 0, \qquad (4)$$

where $\boldsymbol{\mu}$ is a diagonal tensor with components $(\mu_\perp, \mu_\perp, \mu_\parallel)$,

$$\mu_\perp = 1/2 + F_{\text{remote}}^\perp + A, \quad \mu_\parallel = 1/2 + F_{\text{remote}}^\parallel.$$

The heterostructure profile/electrostatic potential $V(\mathbf{r})$ and the variation of the composition are incorporated into Eqs. (1)–(4) by changing E to $E-V$ (everywhere, not just in the Schrödinger equation) and also explicitly via the material-dependent band-structure parameters (E_g, δ, P, and F_{remote}). Hence, the A and D in the heterostructure become all $\mathbf{r}$ dependent. The placement of the tensor $\boldsymbol{\mu}$ and coefficient D *between* two wave vector differential operators in Eq. (4) accounts properly for these coordinate dependencies and also allows generation of the appropriate boundary conditions. In particular, the $\hat{\sigma}_z D$ term is especially interesting: with an incorrect order of the operators, it would be always exactly zero. Even with a correct order of the operators, it diminishes when D is constant in real space (this happens in the bulk material). Thus, the $\hat{\sigma}_z D$ term can play a role only in the biased structures and at the heterointerfaces (through the boundary conditions).

The first boundary condition is traditionally[17] chosen to require continuity of the function $\hat{u}$; the second one inarbitrarily follows from Eq. (4) and requires continuity of

$$\mathbf{N}\cdot\{\boldsymbol{\mu}\cdot\mathbf{k}\hat{u} - i\hat{\sigma}_z D[\mathbf{1}_z\times\mathbf{k}]\hat{u}\} \qquad (5)$$

at an interface with a normal $\mathbf{N}$. Here we write the expression compactly in a vector form with a help of a unit vector in the z direction $\mathbf{1}_z$. It is worth mentioning that this boundary condition is obviously *spin dependent* due to the $\hat{\sigma}_z D$ term which can be nonzero on the *oblique* (with respect to the L axis) interfaces and for the nonzero in-plane wave vectors. For example, for an electron in the (111) L valley where axis z is also parallel to the (111), a common heterostructure grown along (001) direction would also form oblique interfaces. When an electric field is present in the het-

erolayers, similar spin dependence takes place not only on the interfaces, but also inside layers.

A. QW with infinite barriers

As an important intermediate step, we consider first a single-band spinless electron with the effective mass tensor $\boldsymbol{\mu}$ in the QW of width a with a hard-wall confinement. Orientation of the heterostructure is defined by the angle θ between the valley axis z and the QW growth direction $\mathbf{N}$. For the particular case of the (111) L valley and $\mathbf{N}=(001)$ we get $\cos\theta = 1/\sqrt{3}$ and $\sin\theta = \sqrt{2/3}$. We introduce a new orthogonal coordinate system (x', y, z') associated with the structure as follows: z' is along the structure growth direction $\mathbf{N}$, x' lies in the plane of z and z', and y is the same in both systems and orthogonal to the $(z-z')$ plane [see Fig. 1(d)].

The eigenstates form subbands with energies

$$E_n(k_{x'}, k_y) = \mu_{\text{growth}}k_{z',n}^2 + \mu_{\text{in-plane}}k_{x'}^2 + \mu_\perp k_y^2, \qquad (6)$$

where $k_{z',n} = \pi n/a$, $\mu_{\text{growth}} = \mu_\perp\sin^2\theta + \mu_\parallel\cos^2\theta$, $\mu_{\text{in-plane}} = \mu_\perp\mu_\parallel/\mu_{\text{growth}}$, and n is an integer. Their corresponding eigenfunctions f can be expressed as

$$f = Ce^{i(k_{x'}x' + k_y y + \tilde{k}z')}\begin{cases}\cos(k_{z',n}z') & \text{for odd } n, \\ \sin(k_{z',n}z') & \text{for even } n.\end{cases} \qquad (7)$$

Here $\tilde{k} = k_{x'}(\mu_\perp - \mu_\parallel)\cos\theta\sin\theta/\mu_{\text{growth}}$ and C is the normalization constant. This more complex form of the quantized states arises because the quantization axis does not coincide with any of the principal axes of the effective mass tensor. Nevertheless, the most important outcome from this example is that the subband minima are reached at $k_{x'} = k_y = 0$ and the electron wave function for this state accepts a conventional and simple form.

In the framework of the 6×6 $\mathbf{k}\cdot\mathbf{p}$ model, the conduction and valence band envelopes for the two spin-degenerate electron states at the bottom of the ground subband are

$$\hat{u}_s = C\cos(k_{z',n}z')\hat{\alpha}_s,$$

$$\hat{v}_{x,s} = \mu_\perp k_{z',n}\sin\theta\sin(k_{z',n}z')\hat{\alpha}_s,$$

$$\hat{v}_{y,s} = i\hat{\sigma}_z Dk_{z',n}\sin\theta\sin(k_{z',n}z')\hat{\alpha}_s, \qquad (8)$$

where $\hat{\alpha}_s$ denotes columns $\hat{\alpha}_\uparrow = (10)$ and $\hat{\alpha}_\downarrow = (01)$, which are two-component spinors corresponding to spin up and down pure states along the original axis z (and written in the $\hat{\sigma}_z$ basis).

B. QW with finite barriers

Now we turn to the case of a QW with finite interface offsets. Starting from Eq. (5), we readily find an equation for the second boundary condition in the structure frame (x', y, z'), which is continuity of

$$\{\mu_{\text{growth}}k_{z'} + (\mu_\parallel - \mu_\perp)\cos\theta\sin\theta k_{x'} - i\hat{\sigma}_z D\sin\theta k_y\}\hat{u} \qquad (9)$$

at the interface. The $\hat{\sigma}_z D$ term is present for any $\theta \neq 0$, which essentially means that this boundary condition is spin dependent and can potentially result in the splitting of spin states $\uparrow$ and $\downarrow$ at a finite in-plane wave vector k_y manifesting the intrinsic SO effect. We will return to this point later.

Eigenstates of the L electrons characterized by the arbitrary $k_{x'}$, k_y components of the in-plane wave vector should be found numerically as a solution of the transcendental equation in the case of the QW with finite barriers. Similar to the situation of the QW with infinite barrier, subband extrema take place at the zero in-plane momentum which again allows substantial simplifications. Luckily, we are interested in the analysis of the g factor values only at the bottom of the ground subband.

Strain is very important in SiGe heterostructures, since it is the strain-induced shift of the conduction band states that allows formation of the QW confinement potential in the Ge-rich layer. Without that, Ge-rich layer would form a barrier instead. Shifts of the conduction and valence band edges due to strain are easily included into the Eq. (1) and the calculation procedure.

III. TENSOR OF THE ELECTRON g FACTOR

The general procedure how to calculate the g factor tensor in heterostructures is thoroughly described.[12,14] In short, for a pair of states $|s\rangle$ ($s = \uparrow$ or $\downarrow$), the Zeeman contribution to the effective 2×2 Hamiltonian can be expressed as

$$\delta\mathcal{H}_{ss'} \equiv \frac{1}{4c}\boldsymbol{\sigma}_{ss'}\boldsymbol{g}\cdot\boldsymbol{B} \equiv \frac{1}{4c}\sigma_{\alpha,ss'}g_{\alpha\beta}B_{\beta} = \langle s|\delta\mathcal{H}_{\boldsymbol{B}}|s'\rangle$$
$$+ \left\{\left\langle s\left|\frac{\boldsymbol{A}}{c}\frac{\partial\mathcal{H}}{\partial\boldsymbol{k}}\right|s'\right\rangle - \frac{\langle\boldsymbol{A}\rangle}{c}\left\langle s\left|\frac{\partial\mathcal{H}}{\partial\boldsymbol{k}}\right|s'\right\rangle\right\}, \quad (10)$$

where $1/4c$ stands for one half of the Bohr magneton $\mu_B/2$ in atomic units, $\langle\boldsymbol{A}\rangle = \langle s|\boldsymbol{A}|s\rangle$. The first and second terms are due to the explicit ($\boldsymbol{B}$ field directly) and implicit (through the vector potential $\boldsymbol{A}$) magnetic field dependence. The second term inside the curly brackets subtracts the diamagnetic contribution originating from the real-space motion of the charged particle in the crossed electric and magnetic fields. This term becomes zero in a system with a reflection symmetry. All matrix elements should be calculated on the zero-field wave functions $|s\rangle$. Equation (10) can be considered as a definition of the g factor tensor $g_{\alpha\beta}$. Note that its practical usefulness depends on the possibility to evaluate all ancillary matrix elements.

A. Bulk g tensor

In the framework of the two-band model, one can produce the following expressions for the components of the electron g factor in the bulk semiconductor:

$$g_\parallel = g_0 + \Delta g_{\text{remote}}^\parallel + 4D|_{E=0},$$

$$g_\perp = g_0 + \Delta g_{\text{remote}}^\perp. \quad (11)$$

Here the coefficient D, defined in Eq. (3), is evaluated at the bottom of the L valley ($E=0$) to give $4D|_{E=0} = -2P^2\delta/(E_g^2 - \delta^2/4)$. In agreement with the original findings of Ref. 5, we obtain that the g tensor is highly anisotropic, upper valence states L_{3v}' contribute only to the longitudinal component, and, consequently, $g_\perp$ is close to g_0.

B. Magnetic field along the x' direction

For the confined electron state with $k_{x'} = k_y = 0$, the spinor $\hat{u}$ can be presented as

$$\hat{u}_s = f\hat{\alpha}_s, \quad (12)$$

where $f(z')$ is a real scalar function. It satisfies the second-order differential equation

$$-\frac{d}{dz'}\left(\mu_{\text{growth}}\frac{df}{dz'}\right) + (V-E)f = 0, \quad (13)$$

with the adjacent boundary conditions requiring f and $\mu_{\text{growth}}df/dz'$ to be continuous at the heterointerfaces. The spinor components $\hat{v}_x$ and $\hat{v}_y$ can be easily expressed via f with the help of Eq. (2). The straightforward derivation by using Eq. (10) for the magnetic field $\boldsymbol{B}\|x'$ with the vector potential taken in the gauge $\boldsymbol{A} = (0, -z'B, 0)$ yields

$$\delta\hat{\mathcal{H}} = \frac{1}{4c}(\hat{\sigma}_z G_\parallel \sin\theta + \hat{\sigma}_x g_\perp \cos\theta)B, \quad (14)$$

where

$$G_\parallel = g_0 + \Delta g_{\text{remote}}^\parallel + \Delta g,$$

$$\Delta g = -4\int dz'(z' - \langle z'\rangle)D\frac{df^2}{dz'}, \quad \langle z'\rangle \equiv \langle s|z'|s\rangle,$$
$$(15)$$

and the linear-in-B splitting of the two spin states can be described by the effective in-plane g factor

$$g_{\text{in-plane}, \, x'} = \sqrt{G_\parallel^2 \sin^2\theta + g_\perp^2 \cos^2\theta}. \quad (16)$$

Thus, one should essentially evaluate an average of D over a proper electron quantum-confined state in the heterostructure, as given in Eq. (15) (all other terms are constant). Note that f-related Δg contributes only to the $G_\parallel$ component (with a $\sin\theta$ angle dependence in the final expression). Essentially, this reiterates a fact that for the bulk g tensor, only one component of the g factor tensor (i.e., along the L valley axis z) is affected by the interaction with the L_{3v}' valence band.

Another finding worth mentioning is the presence of the spin-dependent diamagnetic contribution in the Δg for $B\|x'$ in asymmetric structures—the $\langle z'\rangle$ term. It appears due to the nonzero in-plane group velocity of the states with $k_{x'} = k_y = 0$

$$\hat{v}_{\text{in-plane}, \, y} = \hat{\sigma}_z \sin\theta \int dz' D\frac{df^2}{dz'}, \quad (17)$$

so one can conclude that the effective 2D electron Hamiltonian in asymmetric structures does contain the linear-in-k_y spin-dependent term[18] $\delta\hat{\mathcal{H}} = \eta\hat{\sigma}_z k_y$ (which is similar in origin to the structure-asymmetry-induced term in III-V heterostructures at the Γ point[19,20]).

C. Magnetic field along the *y* direction

Let us now evaluate the in-plane *g* factor for the magnetic field along the *y* axis. The result is not surprising:

$$\delta\hat{\mathcal{H}} = \frac{1}{4c}\hat{\sigma}_y g_\perp B, \quad g_{\text{in-plane, }y} = g_\perp, \quad (18)$$

which is exactly the bulk transverse *g* factor, as no contribution due to the $\boldsymbol{k}\cdot\boldsymbol{p}$ coupling with the L'_{3v} band is possible for this orientation of the magnetic field (and we neglect whatever effects of quantum confinement on the remote bands).

D. Magnetic field along the *z'* direction

Now we derive an equation for the electron *g* factor when magnetic field is applied along the structure growth axis z'. The perturbation theory and Eq. (10) in particular can be readily applied to a system of finite size. On the contrary, in any extended structure (such as an actual QW) the matrix element of the coordinate x' or y is a poorly defined quantity. One of possible solutions to this obstacle was provided in Ref. 14. This method makes use of the spatially modulated magnetic field (similar to how it was done when calculating the magnetic susceptibility[21]). Let us consider an external magnetic field in the form $\boldsymbol{B} = (B_{z'}e^{ik_y y}, 0, 0)\|z$ with the corresponding vector potential $\boldsymbol{A} = (iB_{z'}e^{ik_y y}/k_y, 0, 0)$, find $\delta\mathcal{H}_{ss'}$ for $|s\rangle$ with $k_y \neq 0$ and go to the limit $k_y \to 0$. For $k_{x'} = 0, k_y \neq 0$, the presentation of Eq. (12) for $\hat{u}_s$ transforms into

$$\hat{u}_s = e^{ik_y y}(\hat{I}f - k_y\hat{\sigma}_z\sin\theta h)\hat{\alpha}_s, \quad (19)$$

where $h(z')$ is also a real function. Here $\hat{I}$ is the 2×2 unity matrix. Let us derive equations for the functions *f* and *h*. As it was mentioned before, in the presence of the electric fields within the layers (or composition grading, which is equivalent for that matter), the $\hat{\sigma}_z D$ term causes spin-dependent mixing on the interfaces as well as inside the heterolayers. For the expansion of Eq. (19), this results in the coupling between *f* and *h*. Up to the terms linear in the small quantity k_y, the function $f(z')$ still satisfies Eq. (13) with the corresponding boundary conditions. Thus, *f* is approximately independent of *h*. To the same accuracy, the function *h* can be found as a solution of the following nonhomogeneous differential equation:

$$-\frac{d}{dz'}\left(\mu_{\text{growth}}\frac{dh}{dz'}\right) + (V-E)h = \frac{dD}{dz'}f. \quad (20)$$

Here *E* is the electron energy at $k_y = 0$. In the same first order in k_y, the boundary conditions for $\hat{u}$ can be satisfied, requiring continuity of *h* and the combination of functions *f* and *h*: $\mu_{\text{growth}}(dh/dz') + Df$.

Evaluating Eq. (10), we arrive in the limit of $k_y \to 0$ at the final expression for g_{growth} in the SiGe QW at the *L* point

$$\delta\hat{\mathcal{H}} = \frac{1}{4c}(\hat{\sigma}_z G_\| \cos\theta - \hat{\sigma}_x g_\perp \sin\theta)B, \quad (21)$$

where[22]

$$G_\| = g_0 + \Delta g_{\text{remote}}^\| + \Delta g,$$

$$\Delta g = 4\int dz'\left[Df^2 + A\sin^2\theta\frac{d}{dz'}(fh)\right]. \quad (22)$$

Thus,

$$g_{\text{growth}} = \sqrt{G_\|^2\cos^2\theta + g_\perp^2\sin^2\theta}. \quad (23)$$

When comparing Eqs. (23) and (16), one would immediately notice an exchange of $\cos\theta$ and $\sin\theta$ terms due to $\pi/2$ difference in the orientation of the magnetic field. But that is not all! We would like to draw an attention to the fact that Eqs. (15) and (22) for Δg do differ which is a consequence of overall reduced system symmetry (in comparison to the bulk) which we induce with heterostructure potential/interfaces and/or biased regions. It is exactly the same effect that makes the Γ electron *g* factor anisotropic in the III-V heterostructures,[10] despite the fact that the constituent bulk semiconductors are characterized by the isotropic *g* factor.

E. Arbitrary direction of the magnetic field

With the effective 2×2 Zeeman Hamiltonian $\delta\hat{\mathcal{H}}$ found for the three orthogonal directions of the external magnetic field, generalization to the case of arbitrarily oriented magnetic field is straightforward.

IV. PARAMETERS

The most serious problem shadowing the reliability of the eigenstate calculations in SiGe heterostructures is the lack of a proven complete set of the band structure parameters. We have worked through the available data delivered by the experiment along with the first-principle calculations as presented in our data set compilation of Table I (for pure Si and Ge). Unless otherwise is mentioned explicitly, the data is taken from Ref. 23. We provide the definition of the quantities [referred to Fig. 1(c)] as well as the comment on the parameter evaluation scheme for the SiGe solid solution.

For most of the parameters (called "basic" here), we use the simple linear interpolation for the SiGe solid solutions. This group contains all band gaps, interband matrix elements, etc. Rigorously, one also needs the bowing constants of the interpolation curves but unfortunately those are mostly unavailable (for very rare exceptions, we specifically mention such cases in the text). On the other hand, some parameters are evidently model derivatives (such as, for example, effective masses and *g* factors) and defined by a subset of basic quantities. As they are not expected to follow a linear interpolation law, we denote them "composite" and apply a

TABLE I. Band structure parameters for Si and Ge as well as the type of the interpolation procedure for the SiGe compounds. Unless the source for the particular parameter is cited explicitly in the text, the data is taken from Ref. 23.

	Si	Ge	SiGe
E_{av} (eV)	-7.03	-6.35	linear
Δ_{SO}^{Γ} (eV)	0.044	0.29	linear
$E_{L_{1c}}$ (eV)	2.04	0.744	linear
$E_{L_{3v}}$ (eV)	-1.2	-1.53	linear
$\delta \equiv \Delta_{SO}^{L}$ (eV)	$(2/3)\Delta_{SO}^{\Gamma}$	0.23	linear
$m_{\parallel}$ $[F_c]$	1.418	1.349	composite
$m_{\perp}$ $[P, F_c]$	0.130	0.0791	composite
$g_{\parallel}$ $[\Delta g_{remote}^{\parallel}]$		0.82	composite
$g_{\perp}$ $[\Delta g_{remote}^{\perp}]$		1.93	composite
a_0 (Å)	5.425	5.645	Eq. (24)
c_{11} (10^{12} dyn/cm)	1.675	1.315	linear
c_{12} (10^{12} dyn/cm)	0.65	0.494	linear
c_{44} (10^{12} dyn/cm)	0.801	0.684	linear
$a_{L_{1c}}$ (eV)	-1.7	-0.9	linear
$a_{L_{3v}}$ (eV)	1.4	1.4	constant

different approach. We use the model formulation to utilize their experimentally determined values and extract the data for the yet-to-be-known more basic quantities (they are listed in the first column of Table I in the square brackets). Then the procedure of linear interpolation is applied to those basic quantities for SiGe alloys. Whenever needed, we reconstruct the necessary composite quantity for the particular alloy from the interpolated basic parameters.

Whenever the reference data for one of the parameters is controversial or nonexistent, we test the sensitivity of the electron state and g factor equations to this particular parameter. In this way, we can identify the most critical quantities and minimize the possible error by a more careful selection. A further discussion on these issues is provided below as we go through the list of the material parameters.

For the band line up, we use the model-solid theory which is well described in Ref. 24. The average potential for each SiGe layer is calculated as a linear interpolation between its values for Si and Ge. Δ_{SO}^{Γ} is the SO splitting of the upper valence band Γ_{25}', that, together with E_{av}, defines absolute energy positions of heavy/light hole (Γ_{8v}) and SO-splitted bands (assumed linear). $E_{L_{1c}}$ and $E_{L_{3v}'}$ are energy positions of the lowest conduction band and upper valence band (neglecting SO splitting) at the L point with respect to the Γ_{8v} band (both assumed linear, which is only approximately correct; at the same time, a linear approximation for the principal band gap at the L point $E_g \equiv E_{L_{1c}} - E_{L_{3v}'}$ is believed to be reasonable[25]). With the SO interaction at the L point included, L_{3v}' states are split into two doublets separated by $\delta \equiv \delta_{SO}^{L_{3v}'}$ (assumed linear). This splitting is known for Ge, while for Si we traditionally[5] choose it to be about $(2/3)\Delta_{SO}^{\Gamma}$. Setting this value to be exactly zero (again, the SO interaction is altogether small in Si) has negligible effect on the result of our calculation. Components of the effective

mass tensor in the conduction band at the L point are model derivatives (*composite*) defined by the $\boldsymbol{k} \cdot \boldsymbol{p}$ interactions with the nearby bands. Knowing independently the relevant energy gaps, we use these values to derive the strength of the $\boldsymbol{k} \cdot \boldsymbol{p}$ coupling with the closest L_{3v}' band (P) as well as to estimate the contribution of the remote bands to the effective mass at L_{1c} (F_c). For both P and F_c, we assume linear dependence on the alloy Ge fraction.

Measurements of the Zeeman effect on the bulk L electrons (typically, donor bound) in strained Ge allowed an accurate determination of the bulk g factor tensor (the components $g_{\parallel}$ and $g_{\perp}$).[8,9,16] As these quantities are defined by the $\boldsymbol{k} \cdot \boldsymbol{p}$ interactions with the nearby SO-split bands, we treat them as "composite." Along with the knowledge of the band gap and interband momentum matrix element for the L_{3v}' states, we can estimate contribution of the remote bands to the bulk g factor ($\Delta g_{remote}^{\parallel}$ and $\Delta g_{remote}^{\perp}$). For obvious reasons (i.e., the lowest electron states are at the X point), no such knowledge is available for the L point in Si. We decided to use the Ge values of $\Delta g_{remote}^{\parallel}$ and $\Delta g_{remote}^{\perp}$ for any SiGe composition. Another natural assumption that $\Delta g_{remote}^{\parallel}$ and $\Delta g_{remote}^{\perp}$ are zero in Si does not noticeably modify the result.

For the lattice constant, we make use of the experimental tabulation including the bowing[26]

$$a_0(x) = x a_0^{Ge} + (1-x) a_0^{Si} - 0.00188 x (1-x) \quad \text{Å}. \quad (24)$$

The elastic moduli c_{ij} define strain in the pseudomorphically grown heterostructures and are assumed here to be linear interpolations for solid solutions. Due to the importance of the strain for the conduction band lineup in the SiGe heterostructures, the conduction band deformation potentials $a_{L_{1c}}$ are often discussed and known in Si and Ge to some accuracy[28-31] (assumed linear). It is worth mentioning that these strain-induced shifts are valley dependent and there are actually two independent energy constants Ξ_d, Ξ_u defining the shift of the electronic energy of the ith valley due to strain.[16,27,32]

On the contrary, the deformation potential $a_{L_{3v}'}$ for the L point valence states are probably the least known part of the parameter set (assumed constant). As a guess for the L_{3v}' states, we use the averaged hydrostatic deformation potential for the valence states at the Γ point in Ge and Si (Ref. 30 supplemented by derivations from Refs. 23, 33, and 34). We also neglect any additional strain-induced splittings of the L_{3v}' states, for the lack of information on the corresponding deformation potentials.

V. RESULTS AND DISCUSSION

As an example of a typical SiGe structure, we consider a three-layer Ge-rich QW $Si_{1-a}Ge_a / Si_{1-x}Ge_x / Si_{1-b}Ge_b$ (which can generally be asymmetric, $a \neq b$). It is assumed grown pseudomorphically on a suitable substrate, which defines the in-plane lattice constant for the whole structure and, consequently, the strain tensor in individual layers.
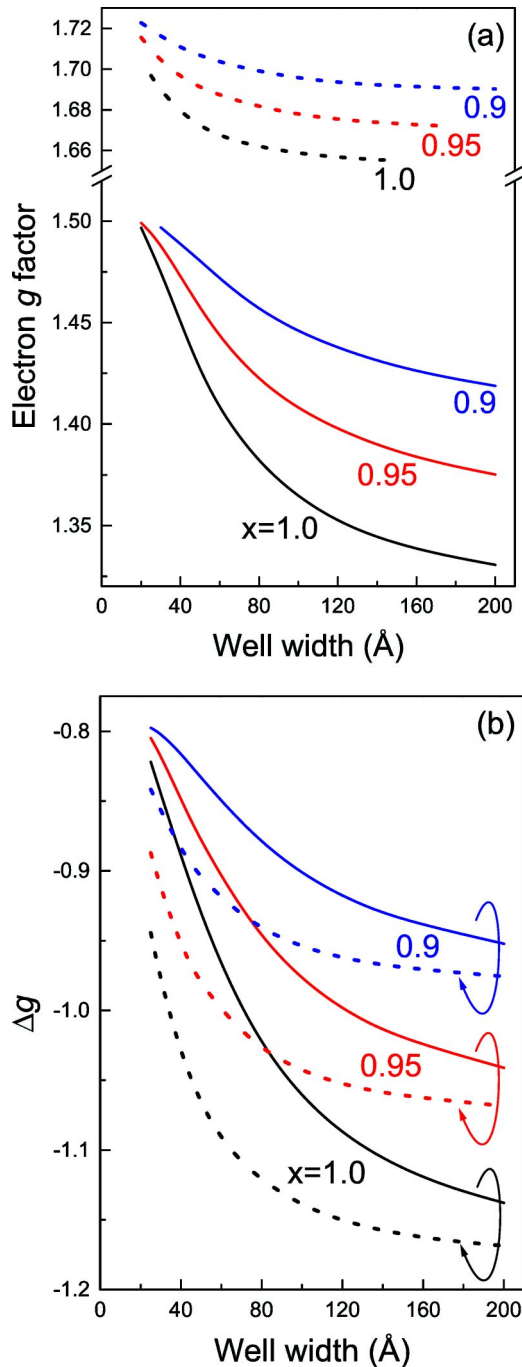
FIG. 2. *g* factor of *L* electron as a function of the QW width. (a) In-plane component (solid lines) of the Lande tensor and the component along the structure growth axis [i.e., (001)] (dashed lines); (b) L'_{3v} SO contribution Δg calculated for the in-plane magnetic field [Eq. (15), solid lines] and along the growth axis [Eq. (22), dashed lines]. The barriers on the left and right are formed by the $Si_{0.3}Ge_{0.7}$ and $Si_{0.2}Ge_{0.8}$, respectively; the Ge content in the QW internal layer is defined by *x*.

A. Effect of composition and quantum confinement

In Fig. 2(a) the components of the *L* electron *g* factor [in-plane (solid lines, lower part) and along the growth direction (dashed lines, upper part)] are given as a function of the QW width for the (001) structure. The two barrier com-

positions are chosen to be different ($a=0.7$ and $b=0.8$). The material of the substrate is assumed to match the lattice constant of one of the barrier layers (for example, this could be a relaxed thick slab of $Si_{1-b}Ge_b$). In case of the sufficiently thick well, both *g* factor components saturate to the respective bulk values of the strained homogeneous material (evaluated along x' and z'). The bulk *g* factor tends to be more positive for higher Si content as a collective effect of larger band gaps, smaller interband momentum matrix element, and weaker SO interaction. Thus, by simply changing the composition of the $Si_{1-x}Ge_x$ internal well layer (lines are shown for $x=0.9$, 0.95, and 1.0), we can substantially modify this asymptotic value. In narrower QW's, quantum confinement effects pick up, making *g* factor even more positive. This manifests to a lesser degree for the growth-direction component [scales for the lower and upper parts of Fig. 2(a) are exactly the same] mostly due to the orientation factors $\sin\theta$ vs $\cos\theta$ in Eqs. (16) and (23). In very narrow QW's, the electron wave function is finally squeezed out of the well layer into one of the barrier regions (whichever is lower), so the bulk *g* factor tensor in that layer now defines the Lande factor of the quantized electron in the whole heterostructure.

As it was mentioned above, for any chosen and fixed θ, whole *g* factor modulation is actually governed exclusively by the L'_{3v}-related SO contribution Δg. Its dynamics is documented in Fig. 2(b) where Δg is calculated for the in-plane magnetic field [Eq. (15), solid lines] and the field applied along the growth axis [Eq. (22), dashed lines]. Although exercising a qualitatively similar behavior, respective solid and dashed lines do not coincide, which is a manifestation of the reduced symmetry (of the heterostructure in comparison to the bulk). Their difference does not exceed 0.1–0.15 (so it is only a small part of the whole SO contribution to the *g* factor) and the maximum is reached in the QW of about 100 Å width. The difference goes down for both wider and narrower wells as the effect of the "asymmetry" of the heterostructure potential on the confined electron declines at both limits.

B. Effect of crystallographic orientation

The crystallographic orientation of the heterostructure has also a profound effect on the Zeeman splitting (see Fig. 3). An extreme anisotropy of both the effective mass tensor and the bulk Lande factor itself are reflected in this strong θ dependence on the orientation as documented by the data sets generated for the (001)-, (011)-, and (111)-grown $Si_{0.3}Ge_{0.7}/Ge/Si_{0.2}Ge_{0.8}$ structures. Not surprisingly, the most flat dependence of the in-plane *g* factor on the QW width is obtained for the (111) structure, where the lowest *L* valley is oriented exactly along the growth direction. This is a very peculiar situation for two reasons: First, it provides the largest effective mass for the spatial confinement (small confinement energy) and, secondly, the in-plane *g* factor is derived exclusively from the transverse component of the bulk *g* tensor. This transverse component is defined by interactions only with remote bands that are not sensitive to the moderate quantum confinement due to the large interband gaps. One
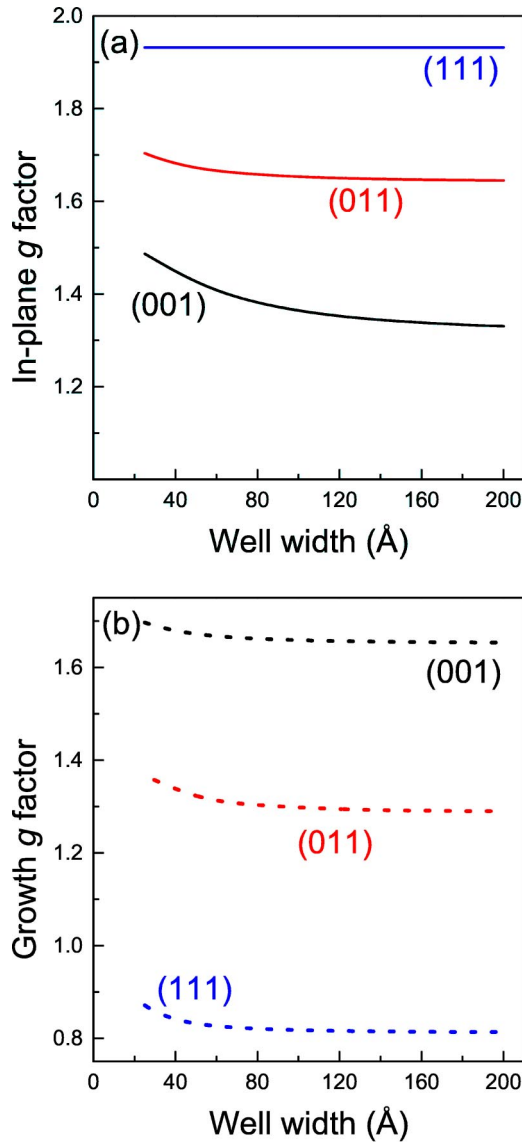
FIG. 3. *g* factor of *L* electron in a SiGe/Ge/SiGe QW for different crystallographic orientations of the heterostructure. (a) In-plane component of the Lande tensor. (b) Component along the structure growth axis.

FIG. 4. *g* factor of *L* electron versus applied electric field: in-plane component of the Lande tensor (solid lines) and the component along the (001) structure growth axis (dashed lines) shown for the 100, 150, and 200 Å QW's.

can see that the effect of spatial confinement is more pronounced in (011) and is the largest in the (001) structure, where the longitudinal bulk *g* factor has the largest contribution. The magnitude of the bulk $g_\parallel$ is substantially smaller than $g_\perp$, which is reflected in the position of (001), (011), (111) lines in Fig. 3(a) with respect to each other. This order is changed to the opposite, when we consider the *g* factor in the growth direction [see Fig. 3(b)]. The strength of the dependence on the well width is also modified by the orientation ($\sin\theta/\cos\theta$ factor).

C. Effect of electric field

Now we turn to the most practically important question of the ability to manipulate *g* factor value in SiGe heterostructure *in situ* with the help of the applied electric field. The
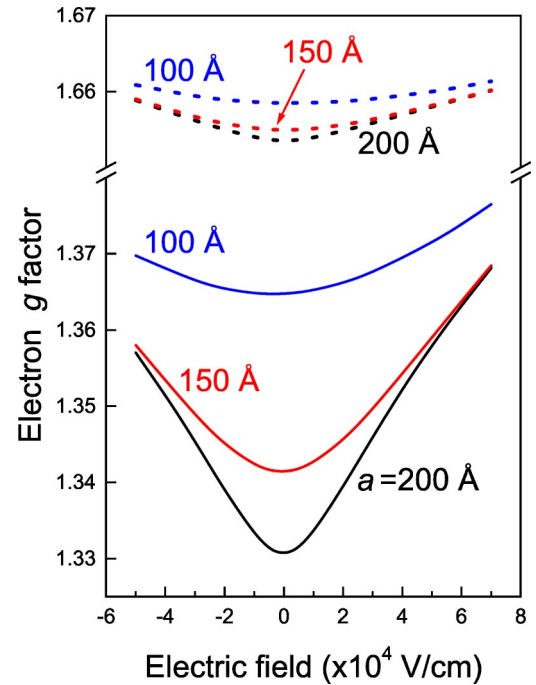
possibility to control *g* factor value by the electric field was originally analyzed in Ref. 11 where the dependence of the Zeeman splitting of electron spin states on the applied bias in III-V QW's had been calculated. The renormalization of the *g* factor value comes mostly from the effect of spatial confinement in the triangular QW at the heterointerface and requires application of relatively high electric fields. At that time, this effect was also observed experimentally by means of the quantum beats spectroscopy in GaAs/Al$_{0.35}$Ga$_{0.65}$As in electric fields up to 9×10^4 V cm^{-1} by Hallstein *et al.*[35] Recent experiments delivered additional confirmations.[3,36] A substantial tunability of the *g* factor was obtained in Ref. 3 by using a heterostructure with a very wide *parabolic* potential profile, allowing large spatial displacement of the whole electron wave function to the layer with a different value of the electron *g* factor.

Figure 4 presents the results of our calculation for SiGe. Here the *L* electron *g* factor in the 100, 150, and 200 Å (001) QW's is shown as a function of the field strength for both positive and negative values. In the first approximation one can neglect the effect of the applied field on the *g* factor component in the growth direction (upper part, dashed lines)—to reinforce this statement, the scales for the upper and low parts of the graph in Fig. 4 are again chosen to be identical. Thus, we will concentrate on the modulation of the in-plane *g* factor component. The main effect of the electric field is to increase the electron quantum confinement by squeezing electron wave function towards the heterointerface, which is also accompanied by the penetration of the electron into the barrier region (with a different, more positive net *g* factor). The effect is small in moderate fields (it

would be exactly quadratic in small fields in a symmetric QW). It is also clear that the overall sensitivity to the small field is higher in thicker QW's where the spatial confinement is weak. A sub-quadratic dependence is obtained in stronger fields. There is a tendency of saturation to a common asymptotic which is independent of the QW width. This happens when the electric field shifts a confined electron towards one of the QW interfaces and finally traps it in the triangular electrostatic potential at the heterojunction, so the spatial position of the second interface has no effect on the trapped electron.[11]

The overall dependence is slightly asymmetric which can be expected for the asymmetric structure. The large asymmetry comes into a play when we discuss the useful range for the applied field. We terminate our curves when substantial leakage of the electron from the QW into the barrier layer starts due to the electric field. As the barriers on the left and right are different, this happens at notably different positive and negative fields. These fields would tend to reduce as the well becomes more shallow (i.e., with increasing content of the Si in the internal layer or increasing Ge content in the barriers). The magnitude of the *g* factor modulation is on the order of a few per cent, consequently, electric manipulation of the *L* electron spin resonance seems to be feasible.

VI. SUMMARY

We developed a consistent theory of the Zeeman effect at the *L* point in SiGe heterostructures. It is based on the ap-propriate $k \cdot p$ model derived for the *L* point states of group IV semiconductors. Effects of the alloy composition, crystallographic orientation, spatial confinement, strain, and electric field are accounted for and documented for an example of the realistic structure design.

Several comments are due. First, the calculation is done for a single valley (out of four). For particular growth orientations, states in two or more valley can be degenerate. As a result, the experiments would measure the *g* factor values averaged over several valleys (as in the case of the previously discussed Zeeman measurements on the donor state in the unstrained bulk Ge providing an isotropic quantity).

Second, so far, the experimental data for some of the SiGe structure parameters have been quite ambiguous. As a new improved set becomes available, our numerical results should be reevaluated in the framework of the current model. The model itself can also be refined to eventually include detailed strain-induced splittings of the valence states when the corresponding deformation potentials are tabulated experimentally.

---

*Electronic address: kiselev@eos.ncsu.edu

[1] D. Loss and D. DiVincenzo, Phys. Rev. A **57**, 120 (1998).

[2] R. Vrijen and E. Yablonovitch, Physica E (Amsterdam) **10**, 569 (2001).

[3] G. Salis, Y. Kato, K. Ensslin, D.C. Driscoll, A.C. Gossard, and D.D. Awschalom, Nature (London) **414**, 619 (2001); Y. Kato, R.C. Myers, D.C. Driscoll, A.C. Gossard, J. Levy, and D.D. Awschalom, Science **299**, 1201 (2003).

[4] R.B. Vrijen, E. Yablonovitch, K.L. Wang, H.W. Jiang, A. Balandin, V. Roychowdhury, T. Mor, and D. DiVincenzo, Phys. Rev. A **62**, 012306 (2000).

[5] L.M. Roth, Phys. Rev. **118**, 1534 (1960).

[6] L. Liu, Phys. Rev. **126**, 1317 (1962).

[7] A. A. Sirenko, T. Ruf, K. Eberl, M. Cardona, A. A. Kiselev, E. L. Ivchenko, and K. Ploog, in *High Magnetic Fields in Semiconductor Physics*, edited by G. Landwehr and W. Ossau (World Scientific, Singapore, 1996), p. 561.

[8] G. Feher, D.K. Wilson, and E.A. Gere, Phys. Rev. Lett. **3**, 25 (1959).

[9] D.K. Wilson and G. Feher, Phys. Rev. **124**, 1068 (1961).

[10] E.L. Ivchenko and A.A. Kiselev, Sov. Phys. Semicond. **26**, 827 (1992).

[11] E.L. Ivchenko, A.A. Kiselev, and M. Willander, Solid State Commun. **102**, 375 (1997).

[12] A.A. Kiselev, E.L. Ivchenko, and U. Rössler, Phys. Rev. B **58**, 16353 (1998).

[13] A.A. Kiselev, E.L. Ivchenko, A.A. Sirenko, T. Ruf, M. Cardona, D.R. Yakovlev, W. Ossau, A. Waag, and G. Landwehr, J. Cryst. Growth **184/185**, 831 (1998).

[14] A.A. Kiselev, K.W. Kim, and E.L. Ivchenko, Phys. Status Solidi B **215**, 235 (1999).

[15] F. Herman, Phys. Rev. **93**, 1214 (1954); Rev. Mod. Phys. **30**, 102 (1958).

[16] H. Hasegawa, Phys. Rev. **118**, 1523 (1960).

[17] E.L. Ivchenko and G.E. Pikus, *Superlattices and Other Heterostructures. Symmetry and Optical Phenomena*, Vol. 110 of *Springer Series in Solid State Sciences*, 2nd ed. (Springer-Verlag, Berlin, 1997).

[18] This term appears in our two-band model exclusively due to the low symmetry of the macroscopic heterostructure potential. Low symmetry of the constituent materials or microscopic structure of the heterointerfaces (or the combination of both) can also lead to similar spin-dependent terms, but that is beyond the competence of our $k \cdot p$ model. For the in-depth group analysis of the latter mechanism for the *L* and *X* states in diamond-lattice heterostructures see L.E. Golub and E.L. Ivchenko (unpublished).

[19] E.I. Rashba, Solid State Phys. **2**, 1109 (1960); Yu.A. Bychkov and E.I. Rashba, JETP Lett. **39**, 78 (1984).

[20] D. Grundler, Phys. Rev. Lett. **84**, 6074 (2000).

[21] J.M. Luttinger and P.J. Stiles, J. Phys. Chem. Solids **17**, 284 (1961).

[22] In Eq. (22), we have also dropped a small indirect contribution of the remote bands to the *g* factor generated through the boundary conditions at oblique interfaces.

[23] *Intrinsic Properties of Group IV Elements and III-V, II-VI, and I-VII Compounds*, edited by O. Madelung, Landolt-Börnstein, New Series, Group III, Vol. 22, Pt. A (Springer, Berlin, 1987);

Semiconductors—Basic Data, edited by O. Madelung (Springer, Berlin, 1996).

[24] C.G. Van de Walle, Phys. Rev. B **39**, 1871 (1989).

[25] D. Stroud and H. Ehrenreich, Phys. Rev. B **2**, 3197 (1970).

[26] J.P. Dismukes, L. Ekstrom, and R.J. Paff, J. Phys. Chem. **68**, 3021 (1964).

[27] C. Herring and E. Vogt, Phys. Rev. **101**, 944 (1956).

[28] C.G. Van de Walle and R.M. Martin, Phys. Rev. B **34**, 5621 (1986).

[29] M.V. Fischetti and S.E. Laux, J. Appl. Phys. **80**, 2234 (1996).

[30] C.G. Van de Walle, Phys. Rev. Lett. **62**, 2028 (1988).

[31] I. Balslev, Phys. Rev. **143**, 636 (1966).

[32] J.M. Hinckley and J. Singh, Phys. Rev. B **42**, 3546 (1990).

[33] L.D. Laude, F.H. Pollak, and M. Cordona, Phys. Rev. B **3**, 2623 (1971).

[34] G.S. Cargill III, J. Angilello III, and K.L. Kavanagh, Phys. Rev. Lett. **61**, 1748 (1988).

[35] S. Hallstein, M. Oestreich, W. W. Rühle, and K. Köhler, in *High Magnetic Fields in Semiconductor Physics*, edited by G. Landwehr and W. Ossau (World Scientific, Singapore, 1996).

[36] H.W. Jiang and E. Yablonovitch, Phys. Rev. B **64**, 041307(R) (2001).